Guide to the Supporting Information

This Supporting Information is organized to make the unit-of-inference and robustness checks explicit. Section S1 defines the operational event labels and distinguishes sampling intervals, event-affected observations, and declustered event episodes. Section S2 reconciles optical-only data availability with the smaller merged optical–PM-mass analysis table. Section S3 describes the measurement site, instruments, and derived variables. Section S4 defines the statistical contrasts, background-IQR-standardized effect sizes, bootstrap procedures, and APSD event-declustering logic. Sections S5–S6 report the merged optical–PM-mass effect-size tables, the cascade-impactor label and PM-mass interpretation caveat, and the negative derived-mass audit. Section S7 reports the APSD-derived native-resolution, event-declustered, declustering-threshold, moving-block-bootstrap, and leave-one-episode-out sensitivity results. Sections S8–S9 provide interpretation of the PM-mass–APSD relationship and the sub-100 nm process-context analysis. Section S10 provides the operational-label audit, the complete merged optical–PM-mass sampling-interval inventory, the declustered APSD episode inventory, and diagnostic visualizations of variable screening, event detection versus event typing, and volume-metric sensitivity. The Supporting Information is therefore intended not as a separate result stream or as documentation for a prediction mechanism, but as the audit trail for the main manuscript's distinction between event detection, the screening of event-responsive variables, the refinement of those screened variables into dust–pollen contrasts, timestamp-level contrasts, and event-level inference.

S1 Event classification and event-count logic

The main manuscript separates two retrospective statistical tasks: event detection and event typing. Event detection compares the pooled event-affected class, $E = D \cup P$, with background observations, B, where D denotes dust-affected observations and P denotes pollen-positive observations. Event typing compares dust-affected observations with pollen-positive observations within the event-affected subset. These terms describe contrasts among already labelled observations; they do not define a forecasting method, a real-time classifier, or a prediction mechanism.

Dust-affected sampling intervals were identified using the processed long-range-transported dust-event indicator based on the Finland dust-event inventory described in the main manuscript.[22] That inventory used MERRA-2 aerosol reanalysis dust column mass density fields followed by multistep verification with independent satellite, aerosol, trajectory, and synoptic evidence. Pollen-positive sampling intervals were identified from SMEAR II cascade-impactor filter records following the approach of Banerji et al.[1] In the merged optical–PM-mass dataset, a row was classified as pollen affected when pollen material was observed on at least one corresponding cascade-impactor size-fraction filter. The complete 2–3 d impactor collection period was then labelled as a pollen-positive sampling interval. This definition includes pollen detected in any measured impactor size fraction; 6 of the 21 pollen-positive intervals were identified solely from pollen detected in the super-PM_{10} fraction. The resulting pollen indicator is therefore an interval-level flag derived from filter evidence, not a pollen concentration or a direct continuous particle-count measurement. The dust and pollen labels were derived from different evidence streams: the dust label represents an externally identified transported-dust period based on a MERRA-2-supported and independently verified long-range transport inventory, whereas the pollen label represents filter-based evidence for pollen material during the impactor sampling interval. In addition, the pollen-positive flag and the PM-mass variables share the cascade-impactor sampling framework in the merged optical–PM-mass dataset. The dust–pollen comparisons are therefore contrasts between two operational event classes rather than a controlled source-apportionment experiment, and PM-mass contrasts are interpreted as response diagnostics rather than independent validation of the pollen label. Background

denotes the non-event reference population at SMEAR II, not aerosol-free or source-free air. In the merged optical–PM-mass dataset, background sampling intervals were intervals classified as neither dust affected nor pollen positive after applying the operational event-label filters. Background observations can therefore still include ordinary boreal aerosol variability from NPF, biogenic emissions, meteorology, transport, and other unclassified sources.

No dust–pollen overlap occurred in the merged optical–PM-mass dataset. Therefore, no priority rule between dust and pollen affected the final event labels.

Three terms are used to distinguish observational units. A *sampling interval* is one 2–3 d cascade-impactor collection period and one row of the merged optical–PM-mass dataset. An *event-affected observation* is a sampling interval or native-resolution APSD observation carrying a dust or pollen label. An *event episode* is a temporally distinct cluster obtained by declustering native-resolution APSD observations. Sampling-interval-level and timestamp-level event labels are not assumed to represent independent atmospheric events. Event-level results refer to comparisons based on declustered episode medians; declustering reduces temporal dependence but does not guarantee complete statistical independence among episodes.

This terminology is used because earlier SMEAR II aerosol particle-size-distribution studies classified observations into event and nonevent categories, while the underlying aerosol records remained temporally structured.[6, 2, 5] More generally, atmospheric measurement time series commonly exhibit serial dependence, and treating all repeated measurements within one atmospheric episode as independent replicates can overstate the effective sample size.[4] Therefore, the sampling-interval-level and native timestamp-level analyses are interpreted together with event-level sensitivity analyses. The complete labelled sampling-interval inventory and the complete declustered APSD episode inventory are reported in Sect. S10.

Table S1: Final exclusive sampling-interval classifications in the merged optical–PM-mass dataset. These counts are not numbers of calendar days or statistically independent atmospheric episodes.

Class	Number of sampling intervals
Background	1545
Pollen-positive	21
Dust-affected	15
Event-affected	36
Total	1581

Table S2: Month distribution of dust-affected and pollen-positive sampling intervals in the merged optical–PM-mass dataset.

Interval classification	Month	Number of sampling intervals
Dust-affected	February	2
Dust-affected	March	3
Dust-affected	April	4
Dust-affected	May	1
Dust-affected	June	2
Dust-affected	July	2
Dust-affected	August	1
Pollen-positive	April	2
Pollen-positive	May	14
Pollen-positive	June	5

S2 Optical-only availability versus merged optical–PM-mass analysis counts

Two analysis-ready data structures were used. The optical-only data tables describe instrumental and optical-data availability. The merged optical–PM-mass dataset was used for like-for-like event-detection and event-typing comparisons involving optical variables and PM-mass variables.

The larger optical-only counts should not be interpreted as the sample size used for the merged optical–PM-mass event statistics in the main manuscript. These optical-only counts are provided only to document instrumental data availability; they are not used as the sample sizes for the merged optical–PM-mass event-detection or event-typing effect sizes.

Table S3 explains why some availability counts are in the 3000–4000 range. These values are valid optical-only observations retained before the additional restrictions imposed by the cascade-impactor PM-mass merge and event-label table. They answer a data-availability question: how many valid optical measurements existed for each optical variable after optical-instrument processing and variable-specific filtering? They do not answer the event-analysis question, because those optical-only records are not all paired with valid PM-mass sampling intervals and final event labels in the merged optical–PM-mass dataset. Therefore, the values in Table S3 are not used as the denominators for the event–background or dust–pollen effect-size tables in the main manuscript.

Table S3: Optical-only valid observation counts. These counts describe optical-data availability before restriction to the merged optical–PM-mass event-analysis table; they are not the event-analysis sample sizes.

Variable	Valid observations
PM_1 $\sigma_{sca,550}$	4043
$PM_{1–10}$ $\sigma_{sca,550}$	4019
PM_1 SAE	4043
$PM_{1–10}$ SAE	3981
PM_1 $\sigma_{abs,520}$	3254
$PM_{1–10}$ $\sigma_{abs,520}$	3254
PM_1 AAE	3253
$PM_{1–10}$ AAE	3049
PM_1 SSA_{550}	3198
$PM_{1–10}$ SSA_{550}	3026

Table S4 gives the counts that correspond to the merged optical–PM-mass statistical analyses. The values in the 1500s arise because the event-analysis table is restricted to the 2–3 d cascade-impactor sampling-interval framework and to rows that can be assigned to background, dust-affected, or pollen-positive classes. After this merge, the full labelled table contains 1581 sampling intervals, of which 1545 are background, 15 are dust affected, and 21 are pollen positive before variable-specific missing-value filtering (Table S1). For each variable in Table S4, the "Valid observations" column is the number of merged sampling intervals remaining after that variable's missing values are removed. Thus, PM-mass variables have 1563 valid merged observations, while optical variables such as PM_1 $\sigma_{sca,550}$ and $PM_{1–10}$ $\sigma_{sca,550}$ have fewer valid merged observations because valid optical and PM-mass/event-label information must coexist in the same sampling interval. The Background, Dust, Pollen, and Event columns then show how those valid merged observations are distributed among the operational classes. These values are sampling-interval counts, not independent atmospheric episodes; independent-event sensitivity checks are reported separately for the APSD-derived metrics in Sect. S7.

Table S4: Variable-specific sampling-interval counts by classification in the merged optical–PM-mass dataset. Counts are calculated after variable-specific missing-value filtering and define the sample sizes used for the merged optical–PM-mass event statistics; they do not represent independent event episodes.

Variable	Valid observations	Background	Dust	Pollen	Event
PM_1 mass	1563	1527	15	21	36
PM_{10} mass	1563	1527	15	21	36
$PM_{1–10}$ mass	1563	1527	15	21	36
super-PM_{10} mass	1563	1527	15	21	36
PM_1 $\sigma_{sca,550}$	1481	1447	13	21	34
$PM_{1–10}$ $\sigma_{sca,550}$	1474	1440	13	21	34
PM_1 SAE	1481	1447	13	21	34
$PM_{1–10}$ SAE	1469	1436	13	20	33
PM_1 $\sigma_{abs,520}$	1231	1205	11	15	26
$PM_{1–10}$ $\sigma_{abs,520}$	1231	1205	11	15	26
PM_1 AAE	1231	1205	11	15	26
$PM_{1–10}$ AAE	1205	1180	11	14	25
PM_1 SSA_{550}	1214	1191	9	14	23
$PM_{1–10}$ SSA_{550}	1193	1170	9	14	23
PM_1 MAC_{520}	1202	1176	11	15	26
$PM_{1–10}$ MAC_{520}	1202	1176	11	15	26
PM_1 MSC_{550}	1451	1417	13	21	34
$PM_{1–10}$ MSC_{550}	1441	1407	13	21	34

S3 Measurement site, instruments, and derived variables

S3.1 Measurement site

The measurements used in this study were conducted at SMEAR II (Station for Measuring Ecosystem–Atmosphere Relations II), the Hyytiälä boreal forest station in southern Finland. SMEAR II is a long-term research station designed for continuous measurements of ecosystem–atmosphere exchange, trace gases, meteorology, and atmospheric aerosol properties.[9] The station has been widely used for long-term aerosol number size-distribution, aerosol optical-property, and new-particle-formation studies in a boreal environment.[6, 5, 14, 1]

S3.2 Aerosol optical-property instruments

Aerosol optical properties were derived from in-situ measurements of particle light scattering and light absorption. Long-term aerosol optical measurements at SMEAR II, including size-resolved PM_1, PM_{10}, and supermicron aerosol optical properties, have been described previously.[14, 1] In the present analysis, the main optical variables included the scattering coefficient at 550 nm, $\sigma_{sca,550}$; the absorption coefficient at 520 nm, $\sigma_{abs,520}$; the scattering Ångström exponent (SAE); the absorption Ångström exponent (AAE); the single-scattering albedo at 550 nm, SSA_{550}; the mass absorption coefficient, MAC_{520}; and the mass scattering coefficient, MSC_{550}. Optical variables were analysed separately for the PM_1 and $PM_{1–10}$ size ranges where available. These variables were used to test whether dust-affected and pollen-positive periods produce distinguishable optical responses or whether the optical signatures overlap.

S3.3 PM-mass variables

Size-resolved PM-mass variables were taken from the merged optical–PM-mass analysis table. The PM-mass variables used in the present study were PM_1 mass, PM_{10} mass, $PM_{1–10}$ mass, and super-PM_{10} mass. Here, $PM_{1–10}$ mass denotes the derived mass difference between PM_{10}

and PM_1, and super-PM_{10} mass denotes the derived mass fraction above 10 μm. Because the pollen-positive flag was also derived from cascade-impactor filter evidence, PM-mass contrasts are not interpreted as independent source validation. They are retained because they describe how the labelled event classes differed in the same merged optical–PM-mass analysis framework. Because some PM-mass quantities are subtraction-derived, negative values can occur when the relevant measured or derived quantities are close to their uncertainty limits. The negative-value audit and sensitivity analysis are reported in Sect. S6.

S3.4 Particle size-distribution instruments and APSD-derived metrics

Aerosol particle size distributions were constructed from mobility and aerodynamic particle size-distribution measurements. The fine-particle size range was measured using a differential mobility particle sizer framework, while the larger-particle size range was measured using an aerodynamic particle sizer. This combined DMPS–APS framework is commonly used to describe the particle number size distribution across submicron and supermicron sizes at SMEAR II and related long-term atmospheric aerosol stations.[14, 24, 1] In the present analysis, the merged size distributions were expressed as number size distributions, cross-sectional-area size distributions, and volume size distributions.

The APSD-derived metrics were calculated from these size distributions to connect the measured particle-size structure with optical and mass responses. The main derived metrics were accumulation-mode cross-sectional area, S_{acc}; accumulation-mode volume, V_{acc}; coarse-mode volume, V_{coarse}; the volume-ratio metric, R_V; and Aitken-mode number concentration, N_{Ait}. The number distribution emphasizes particle abundance, the cross-sectional-area distribution emphasizes scattering-relevant particle geometry, and the volume distribution provides a closer link to particle mass for particles of comparable density and morphology.[17] Because mobility and aerodynamic instruments characterize particle size using different equivalent diameters, the APSD-derived area and volume metrics should be interpreted as operational size-distribution metrics unless aerodynamic diameters are converted to geometric or volume-equivalent diameters using explicit density and shape assumptions.

The optical, PM-mass, and APSD-derived datasets differ in time resolution, data availability, and filtering history. Therefore, the main manuscript distinguishes between optical-only availability, merged optical–PM-mass event-analysis counts, and native-resolution APSD-derived metric counts. The optical-only counts describe instrumental data availability, whereas the merged optical–PM-mass counts are used for like-for-like event-detection and event-typing comparisons involving optical and PM-mass variables. The APSD-derived metrics are analysed at native time resolution and are therefore interpreted together with temporal-dependence sensitivity checks.

S4 Statistical definitions and unit of inference

S4.1 Purpose of the statistical audit

Because many aerosol variables were right-skewed and contained occasional large values, continuous variables were summarized using medians and interquartile ranges (IQRs). This median-based, non-parametric emphasis is consistent with long-term SMEAR II aerosol event analyses and with the broader need to account for non-normal, temporally dependent atmospheric measurement series.[6, 2, 5, 4] The principal contrasts were expressed as differences between group medians. The statistical objective was descriptive and inferential: to quantify event–background responses and dust–pollen tendencies, their uncertainty, and their sensitivity to temporal dependence. It was not to train or validate a predictive classifier.

The framework was used as an evidence audit rather than as an automated decision rule. This distinction is important because the labelled data combine operational event indicators, unequal event counts, variable-specific missing values, and repeated observations from temporally

coherent atmospheric episodes. The effect-size tables, confidence intervals, event-declustering checks, moving-block-bootstrap checks, and leave-one-episode-out diagnostics are therefore meant to answer three linked questions: which variables respond to labelled event occurrence, which variables from this screened event-responsive set also retain a dust–pollen contrast, and which apparent contrasts remain too uncertain or too dependent on a small number of episodes to support source-specific interpretation. This structure also makes the analysis reusable: future studies can apply the same contrasts to other stations, years, or aerosol event types before attempting transferability tests or predictive classification.

S4.2 Standardized effect sizes and dominance statistics

For each measured or derived variable X, event detection was defined as the comparison between the pooled event-affected class and background:

$$\Delta^*_{\mathrm{det}}(X) = \frac{\mathrm{median}(X|E) - \mathrm{median}(X|B)}{\mathrm{IQR}(X|B)}. \tag{S1}$$

Dust–pollen typing was defined as:

$$\Delta^*_{\mathrm{typ}}(X) = \frac{\mathrm{median}(X|D) - \mathrm{median}(X|P)}{\mathrm{IQR}(X|B)}. \tag{S2}$$

Here, E is the pooled event-affected class, B is background, D is the dust-affected class, and P is the pollen-positive class. Dividing by the background IQR places effects from variables with different units and ranges on a comparable scale. Positive typing values indicate larger values in the dust-affected class, whereas negative typing values indicate larger values in the pollen-positive class. In the merged optical–PM-mass analysis, these classes consist of classified sampling intervals; in the event-level APSD analysis, they consist of declustered episode medians.

Cliff's δ was used as a non-parametric effect-size measure:[3, 23]

$$\delta = \frac{\#(x_i > y_j) - \#(x_i < y_j)}{n_x n_y}. \tag{S3}$$

S4.3 Merged optical–PM-mass bootstrap uncertainty

For the merged optical–PM-mass analysis, the classified sampling interval was the observational unit. Confidence intervals for median differences were calculated using 5000 block-bootstrap resamples.[8, 13] Contiguous day blocks were resampled to preserve temporal dependence within sampling periods. A data-driven procedure selected the block length separately for each particle-size fraction and feature set using the sampling-interval duration and decay of the background autocorrelation function, with the selected length constrained to 1–3 d. The word pseudo-daily refers only to this resampling grid. The underlying observations remain the 2–3 d cascade-impactor sampling intervals used in the supermicron aerosol framework of Banerji et al.;[1] the calendar-day blocks are used only to keep adjacent intervals together during bootstrap resampling and should not be read as independent daily measurements. Mann–Whitney tests were used as supporting non-parametric distributional tests.[15] Because the analysis considered several related optical, PM-mass, and APSD-derived variables, the tables should be read as effect-size and robustness summaries rather than as a variable-selection exercise based on isolated p values. The PM-mass results should also be read with the operational-label caveat in Sect. S1: they are response diagnostics for the labelled event set, not independent source-validation tests.

S4.4 APSD anomaly correction and event declustering

For native-resolution APSD-derived metrics, month anomalies were calculated by subtracting the corresponding background calendar-month median, and month-plus-hour anomalies were

calculated by subtracting the corresponding background calendar-month and hour median. Month-plus-hour anomalies were the preferred temporal correction. The preferred Pool B background was restricted to 2011–2014 because all pollen-positive observations occurred within this period, reducing confounding from longer-term differences in data coverage. A stricter common-support-year baseline was used as a sensitivity check.

Native-resolution APSD observations within event-affected periods are repeated, time-correlated measurements. Timestamp-level month-plus-hour anomalies were therefore declustered into event episodes, with a new episode defined operationally when the gap between consecutive observations was at least 48 h. The 48 h threshold is a conservative run-declustering choice rather than a physical lifetime for dust or pollen events. Similar event-sequence and run-declustering logic is used in atmospheric extreme-event and dust-event studies where closely spaced records can belong to the same evolving atmospheric episode.[21, 18] One median anomaly represented each episode, yielding 15 dust episodes and 8 pollen episodes. These declustered episode medians were treated as the event-level units of inference, but the 48 h rule reduces dependence rather than guaranteeing complete independence. The sensitivity of this operational choice was checked by repeating the declustering with 24, 48, and 72 h gap criteria. The 24 h threshold yielded 15 dust and 9 pollen episodes, while the 48 and 72 h thresholds produced identical episode lists with 15 dust and 8 pollen episodes. The 24 h threshold therefore split one additional pollen episode, but all five APSD metrics retained the same dust-minus-pollen median-difference direction across the tested thresholds (Table S12). Event-level confidence intervals were calculated from 2000 balanced bootstrap resamples of the episode medians. As a second sensitivity check, a 24 h moving-block bootstrap with 2000 resamples retained timestamp-level observations while preserving short-term temporal dependence.[13]

S4.5 Evidence hierarchy and interpretation

The APSD evidence was interpreted hierarchically. Native-resolution contrasts describe observed distributional differences but were not treated as primary inferential evidence because many timestamps originated from the same event-affected periods. Greater inferential weight was placed on consistency of effect direction across temporal corrections, declustered episode-level comparisons, and moving-block-bootstrap sensitivity analyses. Very small timestamp-level p values were treated as supporting diagnostics. A confidence interval crossing zero indicates that the data are compatible with no difference and with effects in either direction; it does not establish the absence of a physically meaningful difference. Wide episode-level confidence intervals were interpreted as evidence of substantial uncertainty and limited precision. Given the small number of declustered episodes, especially for pollen, the results are presented as physically interpretable event-type tendencies rather than as a definitive operational classification model.

S5 Merged optical–PM-mass effect-size results

S5.1 Event detection

Table S5: Sampling-interval-level event-detection effect sizes in the merged optical–PM-mass dataset. The contrast is event affected minus background. PM mass is reported in μg m^{-3}; scattering and absorption coefficients are reported in Mm^{-1}; SAE, AAE, and SSA are dimensionless; MAC and MSC are reported in their corresponding mass-normalized coefficient units.

Variable	Δ^*_{det}	Median difference	CI low	CI high	Cliff's δ
PM_1 mass	1.014	2.646	1.555	3.875	0.489
PM_{10} mass	1.414	5.507	3.301	9.567	0.581
$PM_{1–10}$ mass	1.642	2.438	1.283	7.069	0.619
super-PM_{10} mass	3.721	2.918	1.558	5.677	0.712
PM_1 $\sigma_{\mathrm{sca},550}$	0.883	8.046	3.847	12.287	0.463
$PM_{1–10}$ $\sigma_{\mathrm{sca},550}$	0.806	1.823	0.478	2.885	0.342

Table S5: Sampling-interval-level event-detection effect sizes in the merged optical–PM-mass dataset. Continued.

Variable	Δ^*_{det}	Median difference	CI low	CI high	Cliff's δ
PM_1 SAE	0.378	0.156	0.079	0.213	0.284
$PM_{1–10}$ SAE	0.159	0.079	-0.139	0.273	0.060
PM_1 $\sigma_{\mathrm{abs},520}$	0.452	0.552	0.006	1.001	0.277
$PM_{1–10}$ $\sigma_{\mathrm{abs},520}$	0.706	0.086	-0.005	0.137	0.248
PM_1 AAE	-0.224	-0.042	-0.080	0.022	-0.176
$PM_{1–10}$ AAE	0.000	0.000	-0.067	0.161	0.144
PM_1 SSA_{550}	0.723	0.056	-0.004	0.073	0.311
$PM_{1–10}$ SSA_{550}	-0.098	-0.003	-0.012	0.012	-0.028
PM_1 MAC_{520}	-0.483	-0.208	-0.300	-0.041	-0.293
$PM_{1–10}$ MAC_{520}	-0.560	-0.049	-0.059	-0.025	-0.440
PM_1 MSC_{550}	-0.192	-0.287	-0.632	0.365	-0.079
$PM_{1–10}$ MSC_{550}	-0.444	-0.660	-1.152	-0.348	-0.380

S5.2 Dust–pollen typing

Table S6: Sampling-interval-level dust–pollen typing effect sizes in the merged optical–PM-mass dataset. The contrast is dust affected minus pollen positive. Negative values indicate larger values in pollen-positive sampling intervals. PM mass is reported in μg m^{-3}; scattering and absorption coefficients are reported in Mm^{-1}; SAE, AAE, and SSA are dimensionless; MAC and MSC are reported in their corresponding mass-normalized coefficient units.

Variable	Δ^*_{typ}	Median difference	CI low	CI high	Cliff's δ
PM_1 mass	0.408	1.064	-3.593	2.557	-0.060
PM_{10} mass	-0.640	-2.493	-10.263	2.508	-0.283
$PM_{1–10}$ mass	-3.253	-4.830	-7.264	-0.527	-0.435
super-PM_{10} mass	-4.932	-3.867	-9.032	0.105	-0.594
PM_1 $\sigma_{\mathrm{sca},550}$	0.689	6.273	-4.100	12.788	0.275
$PM_{1–10}$ $\sigma_{\mathrm{sca},550}$	0.461	1.044	-1.690	2.876	0.084
PM_1 SAE	-0.071	-0.029	-0.296	0.198	0.048
$PM_{1–10}$ SAE	-0.628	-0.311	-0.646	0.179	-0.338
PM_1 $\sigma_{\mathrm{abs},520}$	0.082	0.100	-1.083	0.798	-0.018
$PM_{1–10}$ $\sigma_{\mathrm{abs},520}$	-0.791	-0.097	-0.191	0.093	-0.248
PM_1 AAE	0.421	0.078	-0.119	0.103	0.079
$PM_{1–10}$ AAE	0.561	0.184	-0.065	0.445	0.377
PM_1 SSA_{550}	0.352	0.027	-0.094	0.095	0.063
$PM_{1–10}$ SSA_{550}	-0.410	-0.013	-0.071	0.013	-0.349
PM_1 MAC_{520}	0.012	0.005	-0.189	0.711	0.224
$PM_{1–10}$ MAC_{520}	0.195	0.017	-0.016	0.113	0.273
PM_1 MSC_{550}	0.869	1.303	-0.173	2.319	0.502
$PM_{1–10}$ MSC_{550}	0.407	0.605	-0.213	1.795	0.407

S6 Negative derived mass-value audit

Negative values occurred only under background conditions for the PM-mass variables listed in Table S7. These negative values are expected to be most relevant for subtraction-derived quantities, especially super-PM_{10} mass. Sensitivity tests excluding negative mass values produced only minor changes in the main effect-size estimates.

Table S7: Negative derived mass-value audit in the merged optical–PM-mass dataset. PM mass is reported in μg m^{-3}.

Variable	Finite values	Negative values	Negative fraction	Negative background	Negative event
PM_1 mass	1563	2	0.0013	2	0
PM_{10} mass	1563	5	0.0032	5	0
$PM_{1–10}$ mass	1563	28	0.0179	28	0
super-PM_{10} mass	1563	69	0.0441	69	0

Table S8: Sensitivity of selected standardized effect sizes to excluding negative mass values.

Variable	Detection retained	Detection excl. negative	Change	Typing retained	Typing excl. negative	Change
PM_1 mass	1.014	1.015	0.001	0.408	0.408	0.000
PM_{10} mass	1.414	1.419	0.005	-0.640	-0.643	-0.003
$PM_{1–10}$ mass	1.642	1.620	-0.022	-3.253	-3.244	0.009
super-PM_{10} mass	3.721	3.584	-0.137	-4.932	-4.811	0.121

S7 APSD-derived metric results

The APSD-derived metrics were analysed at native time resolution. Therefore, their timestamp-level sample sizes are much larger than the merged optical–PM-mass dataset. These measurements are repeated, time-correlated observations within event-affected periods and are not independent event replicates. The native-resolution results are therefore interpreted together with declustered episode-level and moving-block-bootstrap analyses, where available.

The APSD metric units are as follows: S_{acc} is reported in μm^2 cm^{-3}, V_{acc} and V_{coarse} are reported in μm^3 cm^{-3}, R_V is dimensionless, and N_{Ait} is reported in cm^{-3}.

Table S9: Native-resolution APSD-derived metric counts and medians.

Metric	Class	Non-missing values	Median	IQR	Unit
S_{acc}	Background	111014	30.222	42.091	μm^2 cm^{-3}
S_{acc}	Dust	923	71.865	89.542	μm^2 cm^{-3}
S_{acc}	Pollen	1381	49.123	58.809	μm^2 cm^{-3}
V_{acc}	Background	111014	1.199	1.749	μm^3 cm^{-3}
V_{acc}	Dust	923	2.808	3.464	μm^3 cm^{-3}
V_{acc}	Pollen	1381	1.864	2.304	μm^3 cm^{-3}
V_{coarse}	Background	111648	1.204	1.432	μm^3 cm^{-3}
V_{coarse}	Dust	923	1.369	1.489	μm^3 cm^{-3}
V_{coarse}	Pollen	1381	1.383	2.085	μm^3 cm^{-3}
R_V	Background	111014	0.945	1.736	dimensionless
R_V	Dust	923	0.518	1.100	dimensionless
R_V	Pollen	1381	0.714	1.494	dimensionless
N_{Ait}	Background	111364	404.605	525.627	cm^{-3}
N_{Ait}	Dust	923	412.412	455.336	cm^{-3}
N_{Ait}	Pollen	1381	693.805	766.068	cm^{-3}

For S_{acc}, the native-resolution analysis showed a persistent positive dust–pollen contrast under raw, common-year–month, month-anomaly, and month-plus-hour-anomaly comparisons. Under the preferred Pool B month-plus-hour anomaly baseline, the dust-minus-pollen median difference was 25.390 μm^2 cm^{-3}, with a confidence interval of 17.062–31.983 μm^2 cm^{-3} and $\Delta^* = 0.558$. After event declustering, the contrast retained the same positive direction and had a larger standardized effect, but the bootstrap confidence interval crossed zero and was therefore compatible with no episode-level difference and with effects in either direction. Therefore, S_{acc} is interpreted as the strongest APSD-based tendency in this dataset, rather than as a stand-alone source-identification criterion.

Table S10: Pool B month-plus-hour dust–pollen anomaly contrasts for APSD-derived metrics at native timestamp resolution. Pool B uses the 2011–2014 pollen-observation era. The contrast is dust minus pollen. Median differences and confidence intervals are reported in the unit of each metric.

Metric	Dust n	Pollen n	Median difference	CI low	CI high	Cliff's δ	Δ^*	Unit
S_{acc}	923	1381	25.390	17.062	31.983	0.213	0.558	$\mu\mathrm{m}^2\ \mathrm{cm}^{-3}$
V_{acc}	923	1381	1.000	0.686	1.238	0.196	0.520	$\mu\mathrm{m}^3\ \mathrm{cm}^{-3}$
V_{coarse}	923	1381	-0.057	-0.169	0.079	-0.018	-0.036	$\mu\mathrm{m}^3\ \mathrm{cm}^{-3}$
R_V	923	1381	-0.118	-0.190	-0.040	-0.135	-0.064	dimensionless
N_{Ait}	923	1381	-131.553	-177.840	-87.879	-0.137	-0.250	cm^{-3}

For V_{acc}, the raw and native-resolution anomaly analyses indicated higher accumulation-mode volume during dust-affected observations than during pollen-positive observations. Under the preferred Pool B month-plus-hour native-resolution anomaly baseline, the dust-minus-pollen median difference was 1.000 $\mu\mathrm{m}^3\ \mathrm{cm}^{-3}$ with $\Delta^* = 0.520$. The timestamp-level moving-block bootstrap also supported a positive contrast, with a median difference of 1.033 $\mu\mathrm{m}^3\ \mathrm{cm}^{-3}$ and a confidence interval of 0.026–1.969 $\mu\mathrm{m}^3\ \mathrm{cm}^{-3}$. However, after event declustering into episode medians, the dust-minus-pollen median difference was 1.390 $\mu\mathrm{m}^3\ \mathrm{cm}^{-3}$ with $\Delta^* = 0.723$, but the confidence interval crossed zero, from -0.453 to 3.294 $\mu\mathrm{m}^3\ \mathrm{cm}^{-3}$. Thus, V_{acc} supports the accumulation-mode interpretation but is less robust than S_{acc} as an event-type tendency.

For V_{coarse}, the declustered episode-level month-plus-hour anomaly analysis gave the same qualitative conclusion as the native-resolution analysis: the dust–pollen confidence interval crossed zero. The episode-level dust-minus-pollen median difference was -0.698 $\mu\mathrm{m}^3\ \mathrm{cm}^{-3}$, with a confidence interval of -2.180 to 0.903 $\mu\mathrm{m}^3\ \mathrm{cm}^{-3}$ and $\Delta^* = -0.442$, while the timestamp-level moving-block bootstrap also crossed zero. Therefore, V_{coarse} is not interpreted as a robust dust–pollen event-type metric.

For R_V, the native-resolution analysis indicated a small negative dust–pollen contrast. However, after event declustering into episode medians, the Pool B month-plus-hour anomaly contrast was not robust: the dust-minus-pollen median difference was -0.439, with a confidence interval of -1.660 to 0.611 and $\Delta^* = -0.238$. The timestamp-level moving-block bootstrap also crossed zero. Therefore, R_V is interpreted only as weak supporting context and not as a primary dust–pollen event-type metric.

Table S11: Declustered episode-level and moving-block-bootstrap analyses for APSD-derived metrics where available. Declustered results use one episode median after month-plus-hour anomaly correction; declustering reduces temporal dependence but does not guarantee complete independence among episodes. Moving-block results use timestamp-level month-plus-hour anomalies with 24 h blocks. The contrast is dust minus pollen. Median differences and confidence intervals are reported in the unit of each metric.

Metric	Episode diff.	Episode CI low	Episode CI high	Episode Δ^*	Block diff.	Block CI low	Block CI high	Unit
S_{acc}	41.390	-7.028	64.279	0.910	–	–	–	$\mu\mathrm{m}^2\ \mathrm{cm}^{-3}$
V_{acc}	1.390	-0.453	3.294	0.723	1.033	0.026	1.969	$\mu\mathrm{m}^3\ \mathrm{cm}^{-3}$
V_{coarse}	-0.698	-2.180	0.903	-0.442	-0.051	-0.674	0.494	$\mu\mathrm{m}^3\ \mathrm{cm}^{-3}$
R_V	-0.439	-1.660	0.611	-0.238	-0.136	-0.593	0.201	dimensionless
N_{Ait}	-231.405	-477.830	56.167	-0.439	-126.517	-344.962	28.537	cm^{-3}

The 24 h threshold separated one additional pollen episode from the long June 2012 pollen-positive period, increasing the pollen episode count from 8 to 9. The dust episode count remained 15 under all three thresholds. The 48 and 72 h thresholds produced identical dust and pollen episode-start lists. The signs of the median differences were unchanged: S_{acc} and V_{acc} remained positive, while V_{coarse}, R_V, and N_{Ait} remained negative. A separate rerun of the declustering-sensitivity calculation reproduced the saved reference output, including the episode-start lists, within a numerical tolerance of 10^{-9}. This sensitivity check supports the interpretation that the qualitative directions of the episode-median APSD contrasts are not artifacts of the exact 48 h

Table S12: Declustering-threshold sensitivity for APSD-derived Pool B month-plus-hour episode-median anomalies. A new episode was defined when the gap between consecutive event-labelled APSD observations was at least 24, 48, or 72 h. The contrast is dust minus pollen. The primary analysis used 48 h. The 48 and 72 h thresholds produced identical episode lists and therefore identical values in this dataset; the 24 h threshold split one additional pollen episode. The signs of all five episode-median contrasts are unchanged across the tested thresholds.

Metric	Gap (h)	Dust episodes	Pollen episodes	Median diff.	Δ^*	Cliff's δ	Unit
S_{acc}	24	15	9	34.740	0.763	0.363	$\mu\mathrm{m}^2\ \mathrm{cm}^{-3}$
S_{acc}	48	15	8	41.390	0.910	0.350	$\mu\mathrm{m}^2\ \mathrm{cm}^{-3}$
S_{acc}	72	15	8	41.390	0.910	0.350	$\mu\mathrm{m}^2\ \mathrm{cm}^{-3}$
V_{acc}	24	15	9	1.136	0.591	0.407	$\mu\mathrm{m}^3\ \mathrm{cm}^{-3}$
V_{acc}	48	15	8	1.390	0.723	0.383	$\mu\mathrm{m}^3\ \mathrm{cm}^{-3}$
V_{acc}	72	15	8	1.390	0.723	0.383	$\mu\mathrm{m}^3\ \mathrm{cm}^{-3}$
V_{coarse}	24	15	9	-0.184	-0.116	-0.156	$\mu\mathrm{m}^3\ \mathrm{cm}^{-3}$
V_{coarse}	48	15	8	-0.698	-0.442	-0.300	$\mu\mathrm{m}^3\ \mathrm{cm}^{-3}$
V_{coarse}	72	15	8	-0.698	-0.442	-0.300	$\mu\mathrm{m}^3\ \mathrm{cm}^{-3}$
R_V	24	15	9	-0.150	-0.081	-0.230	dimensionless
R_V	48	15	8	-0.439	-0.238	-0.283	dimensionless
R_V	72	15	8	-0.439	-0.238	-0.283	dimensionless
N_{Ait}	24	15	9	-155.645	-0.295	-0.467	cm^{-3}
N_{Ait}	48	15	8	-231.405	-0.439	-0.500	cm^{-3}
N_{Ait}	72	15	8	-231.405	-0.439	-0.500	cm^{-3}

gap criterion, although the small number of pollen episodes still limits precision.

As an influence diagnostic, a leave-one-episode-out sensitivity analysis was applied to the declustered episode medians. One dust or pollen episode was removed at a time, and the dust-minus-pollen median difference was recalculated. For each APSD-derived metric, this produced 23 recalculations, corresponding to removal of each of the 15 dust episodes and each of the 8 pollen episodes. Across the five metrics, the deletion-level audit therefore contained 115 recalculated contrasts. This test evaluates whether the direction of the episode-level contrast is controlled by one individual episode; it is not a replacement for the bootstrap confidence intervals or the moving-block sensitivity analysis.

Table S13: Leave-one-episode-out sensitivity analysis for declustered APSD-derived episode medians. Values are based on Pool B month-plus-hour anomalies. The contrast is dust minus pollen. "Deletion range" is the range of recalculated median differences after removing one dust or pollen episode at a time. "Largest abs. shift" is the largest absolute change from the baseline episode-median difference. A sign-change count of zero indicates that no single episode deletion reversed the direction of the episode-median contrast.

Metric	Baseline diff.	Deletion range	Sign changes	Largest abs. shift	Unit
S_{acc}	41.390	27.916 to 48.581	0	13.474	$\mu\mathrm{m}^2\ \mathrm{cm}^{-3}$
V_{acc}	1.390	1.055 to 1.643	0	0.335	$\mu\mathrm{m}^3\ \mathrm{cm}^{-3}$
V_{coarse}	-0.698	-1.212 to -0.184	0	0.514	$\mu\mathrm{m}^3\ \mathrm{cm}^{-3}$
R_V	-0.439	-0.729 to -0.150	0	0.289	dimensionless
N_{Ait}	-231.405	-307.165 to -155.645	0	75.760	cm^{-3}

The leave-one-episode-out results show that the direction of each declustered episode-median contrast was stable to deletion of any single episode. For S_{acc} and V_{acc}, the contrast remained positive under all deletions. For V_{coarse}, R_V, and N_{Ait}, the contrast remained negative under all deletions. This supports the conclusion that the median-contrast directions are not produced by one influential episode. The largest absolute shifts were tied among seven dust-episode deletions for S_{acc} and V_{acc}, and among all eight pollen-episode deletions for V_{coarse}, R_V, and N_{Ait}. Therefore, the diagnostic is interpreted as evidence for sign stability rather than as identification of a unique influential episode. This result does not remove the limited precision indicated by the event-level bootstrap confidence intervals in Table S11.

Overall, S_{acc} is treated as the strongest APSD-based dust–pollen contrast in this dataset. V_{acc} provides supporting accumulation-mode evidence in the same direction but is less robust

after event declustering. V_{coarse} and R_V are not treated as robust primary event-type metrics. N_{Ait} is treated as process context rather than as a primary dust–pollen typing metric.

S8 Reconciling PM mass and accumulation-mode cross-sectional area

The main manuscript reports that $PM_{1–10}$ mass was higher in pollen-positive than dust-affected sampling intervals in the merged optical–PM-mass dataset, whereas S_{acc} was higher in dust-affected than pollen-positive APSD observations after month-plus-hour background correction. These results are not contradictory because PM mass and cross-sectional area weight the particle size distribution differently.

PM mass is approximately volume-weighted and scales with particle diameter cubed.[17] Therefore, $PM_{1–10}$ mass can be strongly influenced by relatively large supermicron and coarse-tail particles. In contrast, S_{acc} is an accumulation-mode cross-sectional-area metric and scales with particle diameter squared. It is therefore more directly linked to scattering-relevant particle geometry in the accumulation-mode size range. This distinction explains why pollen-positive sampling intervals can show higher $PM_{1–10}$ mass, while dust-affected APSD observations can show higher controlled accumulation-mode cross-sectional area. This is a size-weighting interpretation of two related but non-identical measurement products; it should not be read as a direct chemical, morphological, or density-resolved closure between the PM-mass and APSD datasets.

S9 Sub-100 nm and NPF-related diagnostics: NPF as a process not specific to dust or pollen

The sub-100 nm size range was analysed to determine whether dust and pollen event periods differed in their nucleation- and Aitken-mode particle behaviour. The 100 nm diameter was used as a diagnostic division because it approximately separates the nucleation- and Aitken-mode size range from the larger accumulation- and coarse-mode size range. This division is not interpreted as a strict physical threshold. Rather, it provides a practical way to separate particle sizes most directly associated with new-particle formation (NPF), early growth, and Aitken-mode variability from the larger size range that contributes more strongly to aerosol cross-sectional area, volume, PM mass, scattering, and cloud condensation nuclei (CCN) relevance.

The central interpretation from the sub-100 nm diagnostics is that NPF-like behaviour is not specific to either dust-affected or pollen-positive periods. In this context, this means that NPF-like particle evolution should not be interpreted as a source-specific signature of dust or pollen. Instead, it reflects the balance between process-level drivers that can occur during either event type. These drivers include the production of low-volatility vapours, photochemical activity, boundary-layer evolution, particle growth rate, and losses to the pre-existing aerosol population through condensation and coagulation sinks.[11, 6, 5, 19] Therefore, an event labelled as pollen or dust can coincide with NPF-like behaviour if the local atmospheric conditions favour nucleation and early particle growth, but either event type can also occur without clear NPF-like behaviour if growth is weak or if the pre-existing aerosol sink is large.

This distinction is important for source interpretation. Dust and pollen are event classes defined by source-related or observational criteria, whereas NPF is a microphysical process. Dust-affected periods may increase the pre-existing aerosol surface area and thereby strengthen the condensation or coagulation sink, which can reduce the survival probability of newly formed particles. However, a dust-affected period can also coincide with meteorological or photochemical conditions favourable for NPF. Similarly, pollen-positive periods can coincide with spring or early-summer conditions favourable for biogenic vapour production and photochemistry, and pollen grains can release subpollen particles through rupture or fragmentation under suitable

environmental conditions.[20, 10] However, pollen presence alone does not imply that NPF must occur. Thus, sub-100 nm variability should not be interpreted as a direct source fingerprint of pollen or dust. It is better interpreted as process-level context describing whether nucleation-mode and Aitken-mode particle dynamics were active during the event period.

Raw N_{Ait} was higher in pollen-positive than dust-affected APSD observations, with median values of 693.805 cm^{-3} for pollen, 412.412 cm^{-3} for dust, and 404.605 cm^{-3} for background. However, after month-plus-hour anomaly correction and event declustering, the difference between dust and pollen retained the same direction but was not statistically robust: the episode-level dust-minus-pollen median difference was -231.405 cm^{-3}, with a confidence interval of -477.830 to 56.167 cm^{-3} and $\Delta^* = -0.439$. A timestamp-level moving-block bootstrap gave a similar non-robust result, with a median difference of -126.517 cm^{-3} and a confidence interval of -344.962 to 28.537 cm^{-3}. Thus, N_{Ait} supports the interpretation that pollen-affected periods can be associated with enhanced sub-100 nm particle concentrations, but this contrast is not sufficiently robust after temporal control to be used as a criterion for distinguishing dust from pollen.

Table S14: Summary of N_{Ait} results used to interpret sub-100 nm particle behaviour. The raw difference between pollen and dust provides process context, but the controlled and declustered episode-level results show that N_{Ait} is not a robust metric for distinguishing dust from pollen.

Quantity	Class or contrast	Value
Raw median	Background	404.605 cm^{-3}
Raw median	Dust	412.412 cm^{-3}
Raw median	Pollen	693.805 cm^{-3}
Episode-level median difference	Dust–pollen	-231.405 cm^{-3}
Episode-level CI	Dust–pollen	-477.830 to 56.167 cm^{-3}
Episode-level Δ^*	Dust–pollen	-0.439
Moving-block median difference	Dust–pollen	-126.517 cm^{-3}
Moving-block CI	Dust–pollen	-344.962 to 28.537 cm^{-3}

The interval-resolved sub-100 nm diagnostics are shown in Figures S1–S6. These figures show particle number size distributions (PSD), volume size distributions (VSD), and cross-sectional-area size distributions (ASD) separately for pollen-positive and dust-affected sampling intervals. The Supporting Information figure files are `figure_7.png`, `figure_8.png`, `figure_9.png`, `figure_10.png`, `figure_11.png`, and `figure_12.png`. Together, these figures show that sub-100 nm particle behaviour varies among labelled sampling intervals and that NPF-like behaviour can occur during both pollen-positive and dust-affected periods. Therefore, sub-100 nm behaviour is interpreted as process-level context rather than as a robust stand-alone criterion for distinguishing dust from pollen.

The process-level interpretation is therefore as follows. Pollen-positive and dust-affected periods can modify the aerosol population, but NPF-like sub-100 nm behaviour is controlled by the local balance between precursor vapour supply, particle growth, and removal to the pre-existing aerosol population. Because these controlling factors can occur during either dust-affected or pollen-positive periods, NPF is not treated here as a dust- or pollen-specific source marker. Instead, it is treated as an accompanying aerosol microphysical process that helps contextualize the event environment. CCN relevance is likewise not determined by the event label alone, because CCN activation depends on particle size, hygroscopicity, composition, mixing state, and supersaturation.[7, 16, 12]

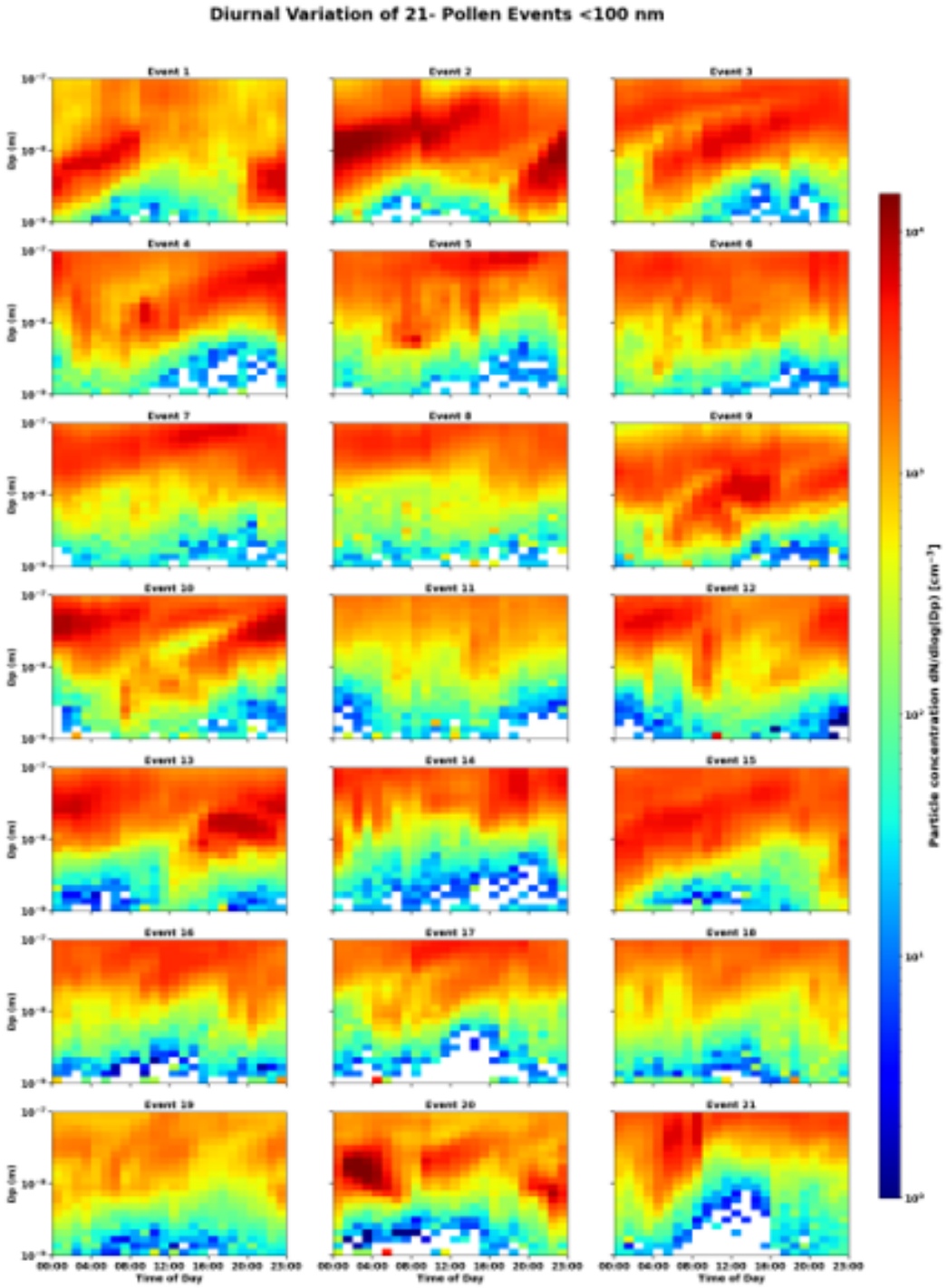

Figure S1: Diurnal variation of sub-100 nm particle number size distributions associated with the 21 pollen-positive sampling intervals. The colour scale shows PSD, $\mathrm{d}N/\mathrm{d}\log(D_p)$, in cm^{-3}. Individual panels show the evolution associated with each labelled sampling interval; they do not represent 21 statistically independent pollen episodes. These interval-resolved PSD panels indicate that pollen-affected periods can be associated with enhanced sub-100 nm particle concentrations, but the timing and structure vary among intervals. Therefore, this figure is interpreted as process-level NPF context rather than as evidence for a pollen-specific NPF signature.

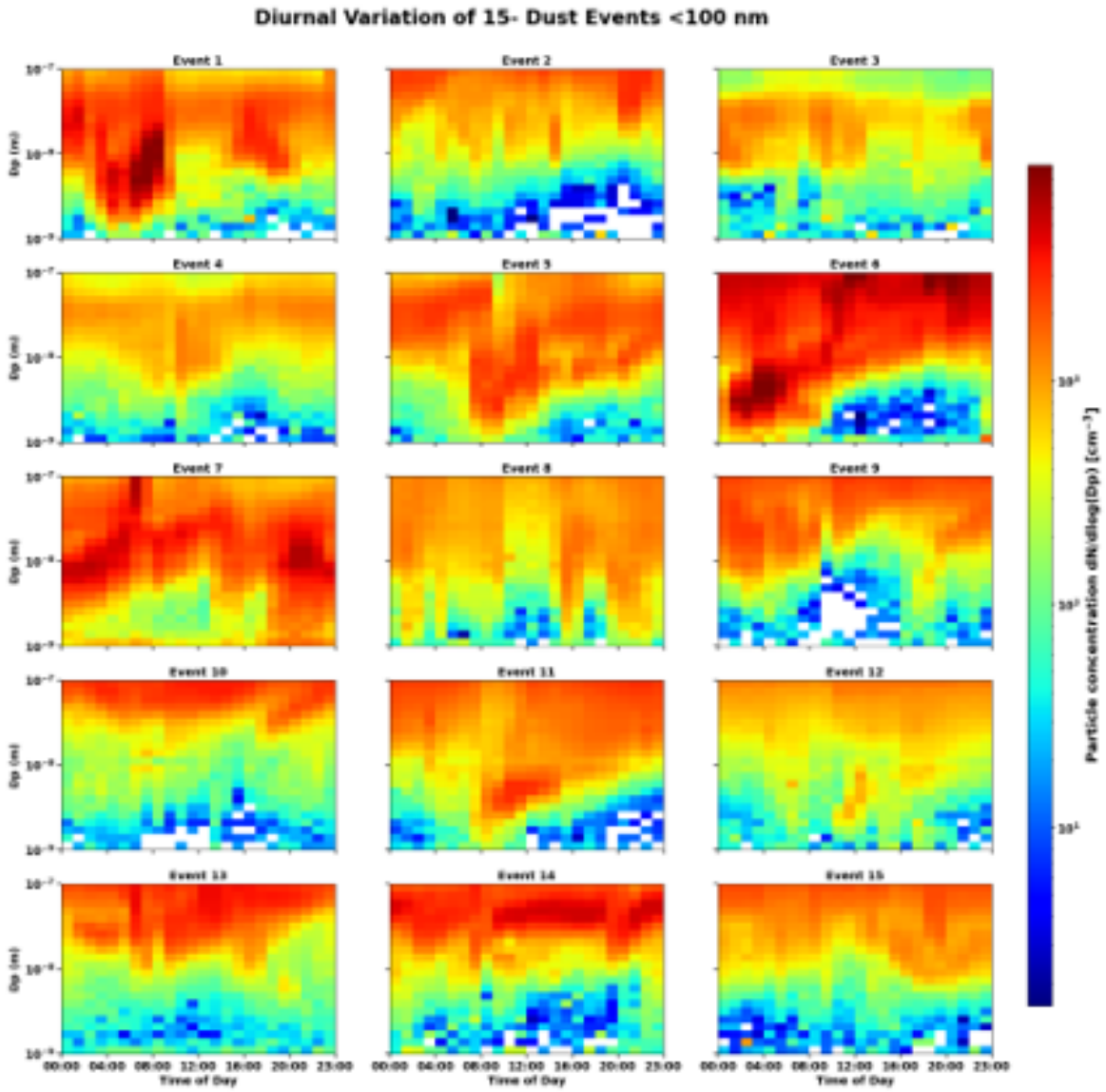

Figure S2: Diurnal variation of sub-100 nm particle number size distributions associated with the 15 dust-affected sampling intervals. The colour scale shows PSD, $\mathrm{d}N/\mathrm{d}\log(D_p)$, in cm^{-3}. Individual panels show the evolution associated with each labelled sampling interval; they do not necessarily represent statistically independent dust episodes. These panels show that sub-100 nm particle structure is also present during some dust-affected periods, supporting the interpretation that NPF-like behaviour is not unique to pollen periods.

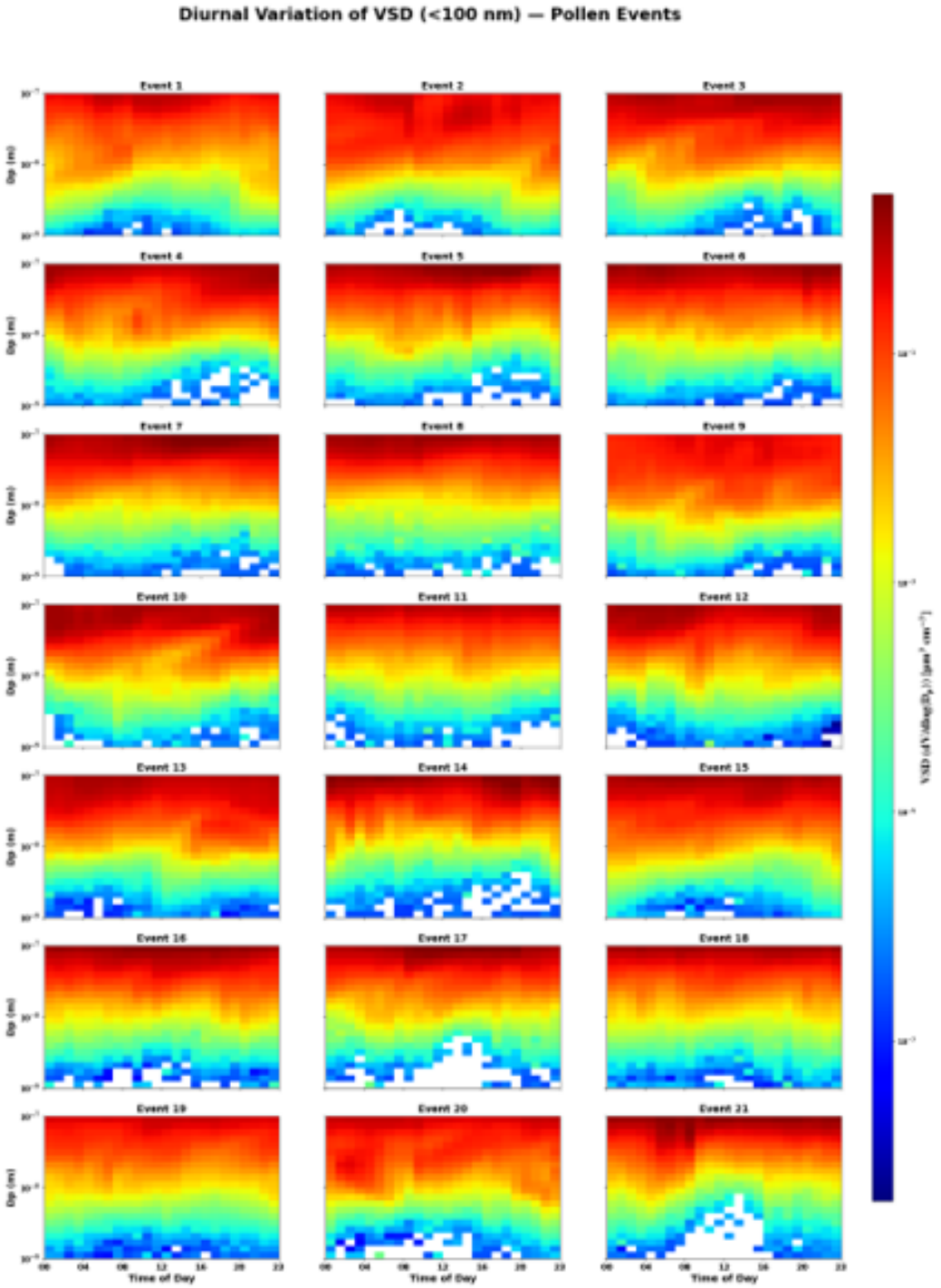

Figure S3: Diurnal variation of sub-100 nm volume size distributions associated with the 21 pollen-positive sampling intervals. The colour scale shows VSD, $\mathrm{d}V/\mathrm{d}\log(D_p)$, in $\mu\mathrm{m}^3$ cm^{-3}. Individual panels correspond to labelled sampling intervals rather than statistically independent pollen episodes. These panels provide volume-weighted context for the pollen-affected sub-100 nm particle population.

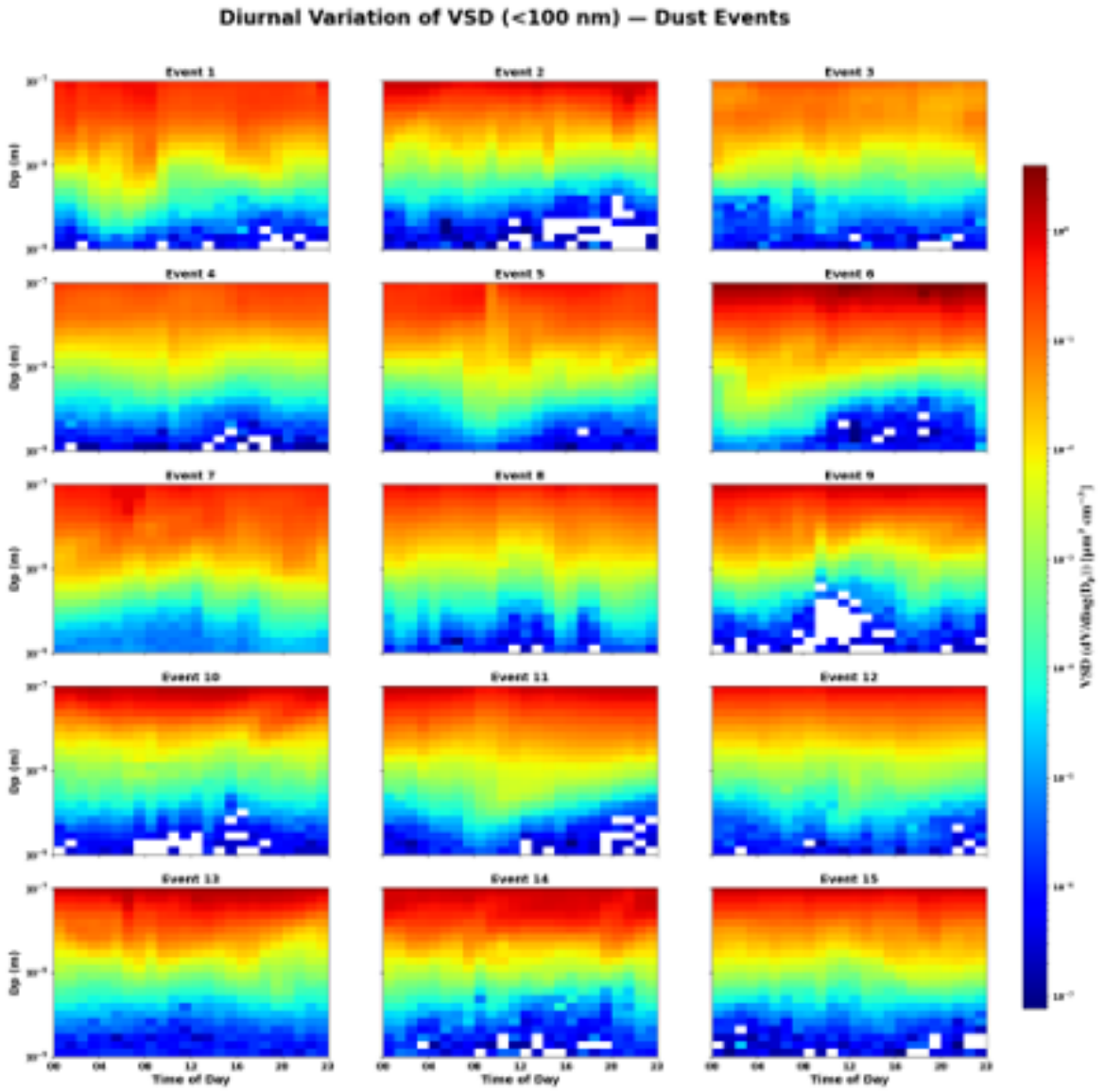

Figure S4: Diurnal variation of sub-100 nm volume size distributions associated with the 15 dust-affected sampling intervals. The colour scale shows VSD, $\mathrm{d}V/\mathrm{d}\log(D_p)$, in $\mu\mathrm{m}^3$ cm^{-3}. Individual panels correspond to labelled sampling intervals rather than necessarily independent dust episodes. These panels provide volume-weighted context for the dust-affected sub-100 nm particle population.

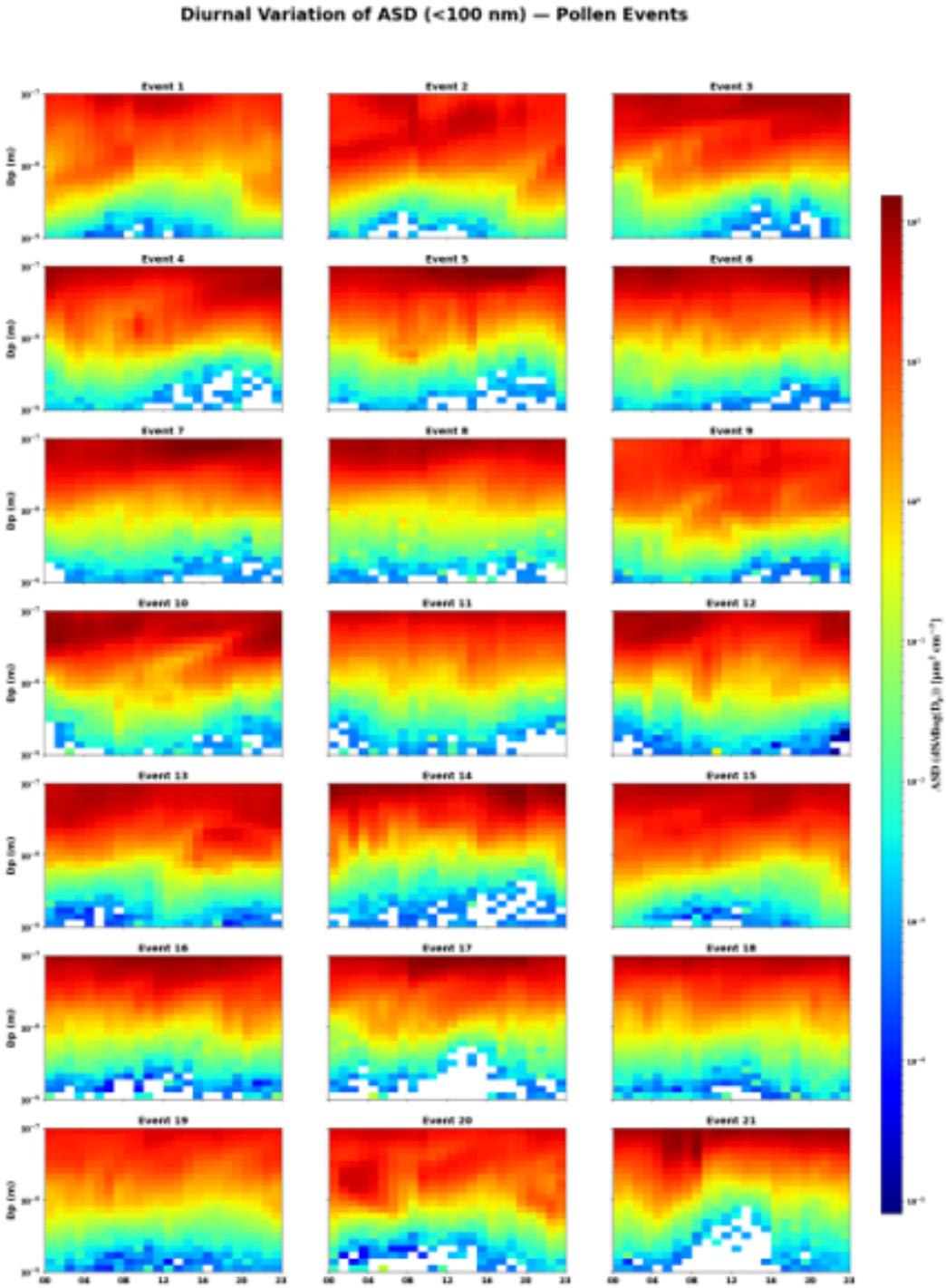

Figure S5: Diurnal variation of sub-100 nm cross-sectional-area size distributions associated with the 21 pollen-positive sampling intervals. The colour scale shows ASD, $\mathrm{d}S/\mathrm{d}\log(D_p)$, in $\mu\mathrm{m}^2$ cm^{-3}. Individual panels correspond to labelled sampling intervals rather than statistically independent pollen episodes. These panels provide area-weighted context for the pollen-affected sub-100 nm particle population.

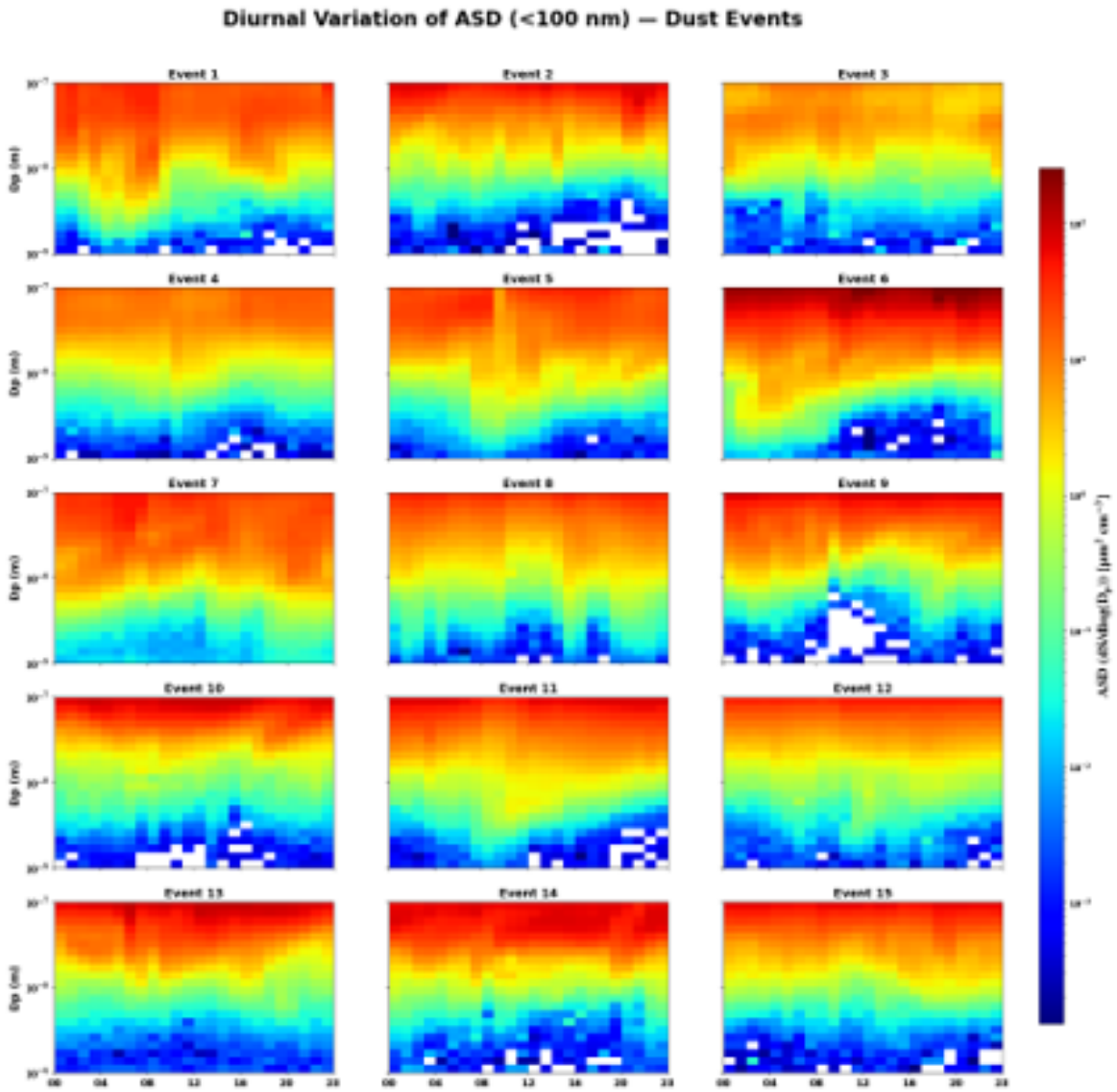

Figure S6: Diurnal variation of sub-100 nm cross-sectional-area size distributions associated with the 15 dust-affected sampling intervals. The colour scale shows ASD, $\mathrm{d}S/\mathrm{d}\log(D_p)$, in $\mu\mathrm{m}^2\ \mathrm{cm}^{-3}$. Individual panels correspond to labelled sampling intervals rather than necessarily independent dust episodes. These panels provide area-weighted context for the dust-affected sub-100 nm particle population.

S10 Event inventories and operational-label audit

This section lists the labelled event observations used in the analyses. Table S15 summarizes how the operational labels were assigned. Table S16 lists the 36 labelled merged optical–PM-mass sampling intervals. Tables S17–S18 list the 23 declustered APSD episodes used for the event-level anomaly analyses. These inventories are included to make explicit that the 21 pollen-positive and 15 dust-affected merged sampling intervals are not the same unit as the 8 pollen and 15 dust declustered APSD episodes.

Table S15: Operational event-label audit. The numerical value 555 is an internal pollen-identification code in the processed cascade-impactor filter records; it is not a measured pollen concentration or a physically meaningful aerosol value. The pollen-positive flag and PM-mass variables share the cascade-impactor sampling framework, so PM-mass contrasts are interpreted as response diagnostics rather than independent source-validation tests.

Label or subset	Evidence stream	Operational rule used in this analysis	Count
Dust-affected sampling interval	Processed transported-dust indicator	`dust_event = 1`; no dust–pollen overlap occurred in the merged optical–PM-mass dataset	15
Pollen-positive sampling interval	Cascade-impactor filter evidence	Pollen code 555 present in at least one corresponding impactor filter flag	21
super-PM_{10}-only pollen subset	Cascade-impactor filter evidence	Pollen code 555 present only in the super-PM_{10} impactor-only flag among the pollen-positive intervals	6
Declustered APSD episode	Native-resolution APSD event labels	A gap of at least 48 h starts a new episode; one median anomaly represents each episode	15 dust; 8 pollen

This audit is included to prevent two possible misinterpretations. First, the 21 pollen-positive and 15 dust-affected merged sampling intervals are labelled observations, not statistically independent atmospheric episodes. Second, the PM-mass variables describe the size-resolved mass response of the labelled event set, but they do not provide independent evidence for the pollen-positive label because both the pollen flag and PM mass are derived from the cascade-impactor sampling framework.

The inventories in Tables S16–S18 also clarify why the apparent event counts differ among analysis layers. The merged optical–PM-mass analysis counts 2–3 d cascade-impactor sampling intervals, giving 21 pollen-positive and 15 dust-affected intervals. The event-level APSD analysis starts from native-resolution APSD observations and then declusters them into temporally separated episodes, giving 8 pollen and 15 dust episodes under the primary 48 h rule. Under the 24 h sensitivity rule, the pollen count increases to 9 because one long pollen-positive period is split into two episodes; under the 72 h rule, the episode list is unchanged from the 48 h rule. The counts answer different questions and are all retained because they correspond to different observational units or sensitivity definitions.

S10.1 Diagnostic visualizations of event detection and event typing

Figures S7–S9 provide diagnostic visualizations of the feature-screening logic used to separate event detection from dust–pollen typing. These figures are not independent hypothesis tests, are not used as stand-alone variable-selection criteria, and do not define an operational classifier. They are included only to show how the numerical effect-size tables, temporal corrections, and physical interpretation combine into the screening hierarchy used in the main manuscript.

Together, these diagnostic figures support the same hierarchy used in the main manuscript. Variables such as super-PM_{10} mass can be strong event detectors, but this does not automatically

Table S16: Complete inventory of the 36 event-affected sampling intervals in the merged optical–PM-mass dataset. The timestamp is the analysis timestamp representing the 2–3 d cascade-impactor collection interval after merging with optical variables. "PM_{10}-range" denotes pollen evidence in the PM_1/$PM_{1–10}$/PM_{10}-related filter flags; "super-PM_{10}" denotes the impactor-only flag above 10 μm.

ID	Class	Timestamp	Month	Label evidence
P1	Pollen	2011-04-16 20:20	Apr	super-PM_{10}-only pollen code
P2	Pollen	2011-04-19 08:33	Apr	super-PM_{10}-only pollen code
P3	Pollen	2011-05-07 19:59	May	super-PM_{10}-only pollen code
P4	Pollen	2011-05-10 08:14	May	super-PM_{10}-only pollen code
P5	Pollen	2011-05-12 09:02	May	super-PM_{10}-only pollen code
P6	Pollen	2011-05-21 19:29	May	PM_{10}-range + super-PM_{10} pollen code
P7	Pollen	2011-05-24 08:23	May	PM_{10}-range + super-PM_{10} pollen code
D1	Dust	2012-04-19 08:12	Apr	transported-dust indicator
P8	Pollen	2012-05-10 08:31	May	PM_{10}-range pollen code
P9	Pollen	2012-05-12 20:06	May	PM_{10}-range + super-PM_{10} pollen code
P10	Pollen	2012-05-22 08:35	May	PM_{10}-range + super-PM_{10} pollen code
P11	Pollen	2012-06-14 07:27	Jun	PM_{10}-range + super-PM_{10} pollen code
P12	Pollen	2012-06-16 19:37	Jun	PM_{10}-range + super-PM_{10} pollen code
P13	Pollen	2012-06-22 19:07	Jun	super-PM_{10}-only pollen code
P14	Pollen	2013-05-30 07:58	May	PM_{10}-range + super-PM_{10} pollen code
D2	Dust	2013-06-01 20:42	Jun	transported-dust indicator
P15	Pollen	2014-05-17 20:08	May	PM_{10}-range + super-PM_{10} pollen code
P16	Pollen	2014-05-20 07:56	May	PM_{10}-range + super-PM_{10} pollen code
P17	Pollen	2014-05-21 19:34	May	PM_{10}-range + super-PM_{10} pollen code
P18	Pollen	2014-05-24 08:21	May	PM_{10}-range + super-PM_{10} pollen code
P19	Pollen	2014-05-29 21:22	May	PM_{10}-range + super-PM_{10} pollen code
P20	Pollen	2014-06-03 08:41	Jun	PM_{10}-range + super-PM_{10} pollen code
P21	Pollen	2014-06-05 07:56	Jun	PM_{10}-range + super-PM_{10} pollen code
D3	Dust	2015-03-26 08:57	Mar	transported-dust indicator
D4	Dust	2016-02-17 09:31	Feb	transported-dust indicator
D5	Dust	2018-04-07 21:05	Apr	transported-dust indicator
D6	Dust	2018-04-14 21:01	Apr	transported-dust indicator
D7	Dust	2019-04-27 20:49	Apr	transported-dust indicator
D8	Dust	2021-02-23 09:07	Feb	transported-dust indicator
D9	Dust	2021-05-18 08:54	May	transported-dust indicator
D10	Dust	2021-06-22 07:30	Jun	transported-dust indicator
D11	Dust	2022-03-17 09:04	Mar	transported-dust indicator
D12	Dust	2022-03-24 09:23	Mar	transported-dust indicator
D13	Dust	2022-07-02 19:58	Jul	transported-dust indicator
D14	Dust	2022-07-12 07:27	Jul	transported-dust indicator
D15	Dust	2022-08-20 19:56	Aug	transported-dust indicator

Table S17: Declustered APSD episode inventory used for event-level month-plus-hour anomaly analyses. Episodes were formed from native-resolution event-labelled APSD observations using a 48 h gap criterion.

Episode	Class	Start	End	Native observations
D1	Dust	2012-04-18 08	2012-04-20 08	49
D2	Dust	2013-05-31 08	2013-06-03 09	74
D3	Dust	2015-03-25 08	2015-03-27 09	50
D4	Dust	2016-02-15 09	2016-02-19 09	97
D5	Dust	2018-04-06 09	2018-04-09 08	72
D6	Dust	2018-04-13 09	2018-04-16 08	72
D7	Dust	2019-04-26 08	2019-04-29 09	74
D8	Dust	2021-02-22 09	2021-02-24 08	48
D9	Dust	2021-05-17 09	2021-05-19 08	48
D10	Dust	2021-06-21 08	2021-06-23 06	47
D11	Dust	2022-03-16 08	2022-03-18 09	50
D12	Dust	2022-03-23 09	2022-03-25 09	49
D13	Dust	2022-07-01 08	2022-07-04 07	72
D14	Dust	2022-07-11 08	2022-07-13 06	47
D15	Dust	2022-08-19 07	2022-08-22 08	74
P1	Pollen	2011-04-15 08	2011-04-20 08	121
P2	Pollen	2011-05-06 08	2011-05-13 09	170
P3	Pollen	2011-05-20 06	2011-05-25 08	123
P4	Pollen	2012-05-09 09	2012-05-14 08	120
P5	Pollen	2012-05-21 08	2012-05-23 08	49
P6	Pollen	2012-06-13 07	2012-06-25 07	243
P7	Pollen	2013-05-29 07	2013-05-31 08	50
P8	Pollen	2014-05-16 08	2014-06-06 08	505

Table S18: Declustered APSD episode-median anomalies under the preferred Pool B month-plus-hour baseline. Units are μm^2 cm^{-3} for S_{acc}, μm^3 cm^{-3} for V_{acc} and V_{coarse}, dimensionless for R_V, and cm^{-3} for N_{Ait}.

Episode	Class	S_{acc}	V_{acc}	V_{coarse}	R_V	N_{Ait}
D1	Dust	10.962	0.551	0.947	0.124	-77.110
D2	Dust	104.046	4.976	0.867	-0.524	-263.619
D3	Dust	3.548	0.077	-0.524	-0.758	-204.520
D4	Dust	-23.732	-1.305	-0.689	0.244	16.433
D5	Dust	-11.145	-0.417	0.614	2.083	-243.339
D6	Dust	46.304	1.566	1.325	-0.381	611.440
D7	Dust	14.509	0.691	2.030	0.480	-63.460
D8	Dust	19.357	0.896	0.029	-0.115	-79.851
D9	Dust	47.362	1.748	0.193	-0.492	-293.349
D10	Dust	118.249	4.886	-0.090	-0.704	-236.329
D11	Dust	66.056	2.558	-0.842	-1.655	-153.822
D12	Dust	116.170	4.821	-1.164	-1.825	-262.362
D13	Dust	55.362	1.778	-0.600	-0.441	17.161
D14	Dust	-41.432	-1.786	-0.354	1.310	298.937
D15	Dust	53.632	2.091	-0.845	-0.745	-148.241
P1	Pollen	-15.605	-0.535	0.094	0.639	-126.452
P2	Pollen	12.106	0.480	1.122	0.288	158.924
P3	Pollen	13.382	0.430	3.751	1.409	323.933
P4	Pollen	-5.687	-0.245	-0.433	-0.291	-85.361
P5	Pollen	-16.883	-0.634	2.091	1.988	679.391
P6	Pollen	-2.277	-0.077	-1.229	-0.609	208.123
P7	Pollen	101.871	4.103	1.184	-0.563	7.404
P8	Pollen	22.598	1.010	-0.314	-0.554	-130.907

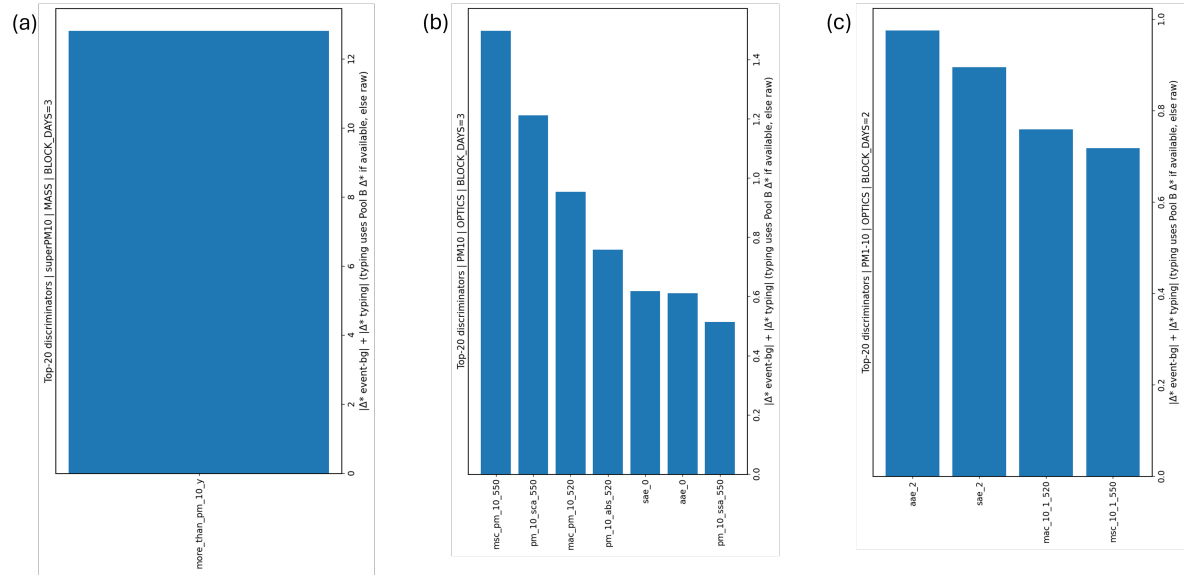

Figure S7: Diagnostic ranking of event-response and dust–pollen-typing variables for selected particle-size fractions and feature families. Bar height represents a combined diagnostic score based on the magnitude of the event–background contrast and the dust–pollen typing contrast. The panels show representative rankings for super-PM_{10} mass, PM_{10} optical variables, and $PM_{1–10}$ optical variables. This figure visualizes the screening logic only; it is not an independent variable-selection procedure or an operational classifier. It should be interpreted together with the effect-size tables, confidence intervals, temporal corrections, and sensitivity analyses.

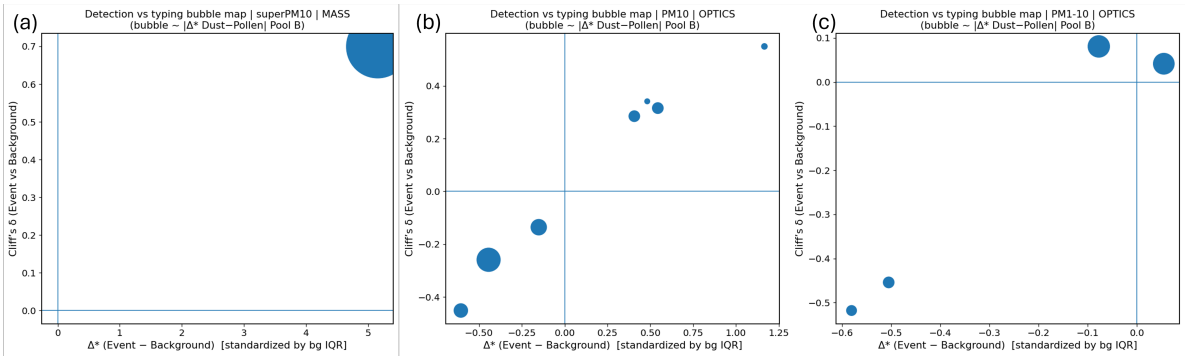

Figure S8: Detection-versus-typing bubble maps for selected particle-size fractions and feature families. The horizontal axis shows the standardized event–background contrast, Δ^*_{det}, and the vertical axis shows Cliff's δ for the event-versus-background comparison. Bubble size is proportional to the absolute dust–pollen typing contrast, $|\Delta^*_{\mathrm{typ}}|$, using the Pool B comparison where available. The figure illustrates that event detection and event typing are related but distinct tasks: a variable may separate event-affected observations from background observations without providing strong dust–pollen separation within the event-affected subset. The bubble maps are descriptive summaries and should not be interpreted as model-training output or classifier performance metrics.

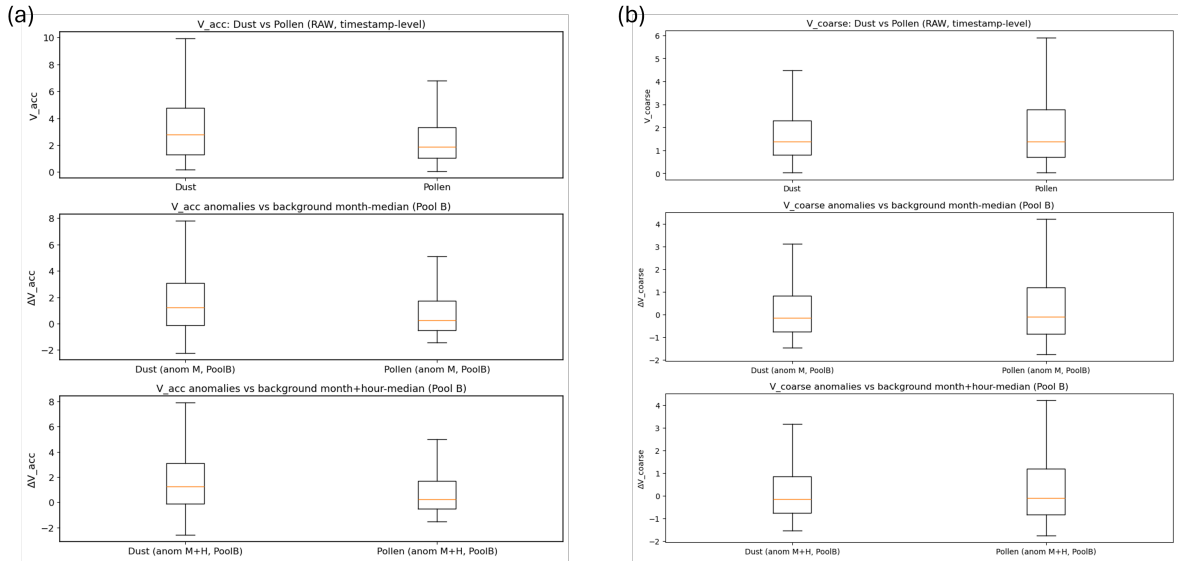

Figure S9: Sensitivity of accumulation-mode and coarse-mode volume metrics to temporal background correction. Panels show raw dust–pollen comparisons, anomalies relative to the background month median, and anomalies relative to the background month-plus-hour median for V_{acc} and V_{coarse}. The V_{acc} panels support a positive dust-minus-pollen accumulation-mode volume tendency after temporal correction, whereas V_{coarse} shows weaker and less consistent separation. These diagnostics support the interpretation that accumulation-mode APSD metrics provide clearer event-type tendencies than coarse-mode volume alone in the present event set, but the event-declustered confidence intervals in Table S11 remain the primary uncertainty check.

make them robust dust–pollen typing variables, especially because the pollen label and PM-mass variables share the cascade-impactor framework. Conversely, accumulation-mode APSD metrics, especially S_{acc} and secondarily V_{acc}, retain clearer dust–pollen tendencies after temporal background correction than coarse-mode volume alone. The numerical interpretation remains based on the effect-size tables, confidence intervals, event-declustered sensitivity checks, moving-block-bootstrap results, leave-one-episode-out diagnostics, and physical size-weighting arguments.

References

[1] Banerji, S.; Luoma, K.; Ylivinkka, I. A. E.; Ahonen, L.; Kerminen, V.-M.; Petäjä, T. Measurement Report: Optical Properties of Supermicron Aerosol Particles in a Boreal Environment. *Atmospheric Chemistry and Physics* **2025**, *25*, 16895–16914. https://doi.org/10.5194/acp-25-16895-2025.

[2] Buenrostro Mazon, S.; Riipinen, I.; Schultz, D. M.; Valtanen, M.; Dal Maso, M.; Sogacheva, L.; Junninen, H.; Nieminen, T.; Kerminen, V.-M.; Kulmala, M. Classifying Previously Undefined Days from Eleven Years of Aerosol-Particle-Size Distribution Data from the SMEAR II Station, Hyytiälä, Finland. *Atmospheric Chemistry and Physics* **2009**, *9*, 667–676. https://doi.org/10.5194/acp-9-667-2009.

[3] Cliff, N. Dominance Statistics: Ordinal Analyses To Answer Ordinal Questions. *Psychological Bulletin* **1993**, *114*, 494–509. https://doi.org/10.1037/0033-2909.114.3.494.

[4] Collaud Coen, M.; Andrews, E.; Bigi, A.; Martucci, G.; Romanens, G.; Vogt, F. P. A.; Vuilleumier, L. Effects of the Prewhitening Method, the Time Granularity, and the Time Segmentation on the Mann–Kendall Trend Detection and the Associated Sen's Slope. *Atmospheric Measurement Techniques* **2020**, *13*, 6945–6964. https://doi.org/10.5194/amt-13-6945-2020.

[5] Dada, L.; Paasonen, P.; Nieminen, T.; Buenrostro Mazon, S.; Kontkanen, J.; Peräkylä, O.; Lehtipalo, K.; Hussein, T.; Petäjä, T.; Kerminen, V.-M.; Bäck, J.; Kulmala, M. Long-Term Analysis of Clear-Sky New Particle Formation Events and Nonevents in Hyytiälä. *Atmospheric Chemistry and Physics* **2017**, *17*, 6227–6241. https://doi.org/10.5194/acp-17-6227-2017.

[6] Dal Maso, M.; Kulmala, M.; Riipinen, I.; Wagner, R.; Hussein, T.; Aalto, P. P.; Lehtinen, K. E. J. Formation and Growth of Fresh Atmospheric Aerosols: Eight Years of Aerosol Size Distribution Data from SMEAR II, Hyytiälä, Finland. *Boreal Environment Research* **2005**, *10*, 323–336. https://www.borenv.net/BER/archive/pdfs/ber10/ber10-323.pdf.

[7] Dusek, U.; Frank, G. P.; Hildebrandt, L.; Curtius, J.; Schneider, J.; Walter, S.; Chand, D.; Drewnick, F.; Hings, S.; Jung, D.; Borrmann, S.; Andreae, M. O. Size Matters More than Chemistry for Cloud-Nucleating Ability of Aerosol Particles. *Science* **2006**, *312*, 1375–1378. https://doi.org/10.1126/science.1125261.

[8] Efron, B.; Tibshirani, R. J. *An Introduction to the Bootstrap*; Chapman & Hall/CRC: New York, 1994. https://doi.org/10.1201/9780429246593.

[9] Hari, P.; Kulmala, M. Station for Measuring Ecosystem–Atmosphere Relations (SMEAR II). *Boreal Environment Research* **2005**, *10*, 315–322. https://www.borenv.net/BER/archive/pdfs/ber10/ber10-315.pdf.

[10] Hendrickson, B. N.; Alsante, A. N.; Brooks, S. D. Live Oak Pollen as a Source of Atmospheric Particles. *Aerobiologia* **2023**, *39*, 51–67. https://doi.org/10.1007/s10453-022-09773-4.

[11] Kerminen, V.-M.; Kulmala, M. Analytical Formulae Connecting the "Real" and the "Apparent" Nucleation Rate and the Nuclei Number Concentration for Atmospheric Nucleation Events. *Journal of Aerosol Science* **2002**, *33*, 609–622. https://doi.org/10.1016/S0021-8502(01)00194-X.

[12] Kerminen, V.-M.; Paramonov, M.; Anttila, T.; Riipinen, I.; Fountoukis, C.; Korhonen, H.; Asmi, E.; Laakso, L.; Lihavainen, H.; Swietlicki, E.; Svenningsson, B.; Asmi, A.; Pandis, S. N.; Kulmala, M.; Petäjä, T. Cloud Condensation Nuclei Production Associated with Atmospheric Nucleation: A Synthesis Based on Existing Literature and New Results. *Atmospheric Chemistry and Physics* **2012**, *12*, 12037–12059. https://doi.org/10.5194/acp-12-12037-2012.

[13] Künsch, H. R. The Jackknife and the Bootstrap for General Stationary Observations. *The Annals of Statistics* **1989**, *17*, 1217–1241. https://doi.org/10.1214/aos/1176347265.

[14] Luoma, K.; Virkkula, A.; Aalto, P. P.; Petäjä, T.; Kulmala, M. Over a 10-Year Record of Aerosol Optical Properties at SMEAR II. *Atmospheric Chemistry and Physics* **2019**, *19*, 11363–11382. https://doi.org/10.5194/acp-19-11363-2019.

[15] Mann, H. B.; Whitney, D. R. On a Test of Whether One of Two Random Variables Is Stochastically Larger than the Other. *Annals of Mathematical Statistics* **1947**, *18*, 50–60. https://doi.org/10.1214/aoms/1177730491.

[16] Petters, M. D.; Kreidenweis, S. M. A Single Parameter Representation of Hygroscopic Growth and Cloud Condensation Nucleus Activity. *Atmospheric Chemistry and Physics* **2007**, *7*, 1961–1971. https://doi.org/10.5194/acp-7-1961-2007.

[17] Seinfeld, J. H.; Pandis, S. N. *Atmospheric Chemistry and Physics: From Air Pollution to Climate Change*, 3rd ed.; John Wiley & Sons: Hoboken, NJ, 2016.

[18] Sarafian, R.; Nissenbaum, D.; Raveh-Rubin, S.; Agrawal, V.; Rudich, Y. Deep Multi-Task Learning for Early Warnings of Dust Events Implemented for the Middle East. *npj Climate and Atmospheric Science* **2023**, *6*, 23. https://doi.org/10.1038/s41612-023-00348-9.

[19] Stolzenburg, D.; Cai, R.; Blichner, S. M.; Kontkanen, J.; Zhou, P.; Makkonen, R.; Kerminen, V.-M.; Kulmala, M.; Riipinen, I.; Kangasluoma, J. Atmospheric Nanoparticle Growth. *Reviews of Modern Physics* **2023**, *95*, 045002. https://doi.org/10.1103/RevModPhys.95.045002.

[20] Steiner, A. L.; Brooks, S. D.; Deng, C.; Thornton, D. C. O.; Pendleton, M. W.; Bryant, V. Pollen as Atmospheric Cloud Condensation Nuclei. *Geophysical Research Letters* **2015**, *42*, 3596–3602. https://doi.org/10.1002/2015GL064060.

[21] Tuel, A.; Martius, O. A Climatology of Sub-Seasonal Temporal Clustering of Extreme Precipitation in Switzerland and Its Links to Extreme Discharge. *Natural Hazards and Earth System Sciences* **2021**, *21*, 2949–2972. https://doi.org/10.5194/nhess-21-2949-2021.

[22] Varga, G.; Meinander, O.; Rostási, Á.; Dagsson-Waldhauserová, P.; Csávics, A.; Gresina, F. Saharan, Aral-Caspian and Middle East Dust Travels to Finland (1980–2022). *Environment International* **2023**, *180*, 108243. https://doi.org/10.1016/j.envint.2023.108243.

[23] Vargha, A.; Delaney, H. D. A Critique and Improvement of the "CL" Common Language Effect Size Statistics of McGraw and Wong. *Journal of Educational and Behavioral Statistics* **2000**, *25*, 101–132. https://doi.org/10.3102/10769986025002101.

[24] Wiedensohler, A.; Birmili, W.; Nowak, A.; Sonntag, A.; Weinhold, K.; Merkel, M.; Wehner, B.; Tuch, T.; Pfeifer, S.; Fiebig, M.; Fjäraa, A. M.; Asmi, E.; Sellegri, K.; Depuy, R.; Venzac, H.; Villani, P.; Laj, P.; Aalto, P.; Ogren, J. A.; Swietlicki, E.; Williams, P.; Roldin, P.; Quincey, P.; Hüglin, C.; Fierz-Schmidhauser, R.; Gysel, M.; Weingartner, E.; Riccobono, F.; Santos, S.; Grüning, C.; Faloon, K.; Beddows, D.; Harrison, R. M.; Monahan, C.; Jennings, S. G.; O'Dowd, C. D.; Marinoni, A.; Horn, H.-G.; Keck, L.; Jiang, J.; Scheckman, J.; McMurry, P. H.; Deng, Z.; Zhao, C. S.; Moerman, M.; Henzing, B.; de Leeuw, G.; Löschau, G.; Bastian, S. Mobility Particle Size Spectrometers: Harmonization of Technical Standards and Data Structure To Facilitate High Quality Long-Term Observations of Atmospheric Particle Number Size Distributions. *Atmospheric Measurement Techniques* **2012**, *5*, 657–685. https://doi.org/10.5194/amt-5-657-2012.